Efficient wavefield inversion in acoustic VTI media applied to field data

Chao Song and Tariq Alkhalifah, King Abdullah University of Science and Technology

SUMMARY

Full-waveform inversion (FWI) is now often used to retrieve high-resolution velocity models in marine datasets. Directly matching the predicted data with the recorded ones at the sensor locations, results in a highly nonlinear optimization problem. Besides its inherent high nonlinearity (manifested in one form in the cycle-skipping problem), considering the anisotropic reality of the true Earth, a multi-parameter inversion imposes additional Null space and the tradeoff issues. To solve these problems, we formulate an optimization problem referred to as an efficient wavefield inversion (EWI) to retrieve multi-parameters. EWI uses background models to reconstruct the wavefield efficiently by introducing an enhanced source function (which includes secondary sources). In this setup, the inversion for the wavefield is linear and efficient. The anisotropic parameters are inverted in a separate direct optimization using the wavefield and the enhanced source function in an efficient matter (no modeling involved). We demonstrate the effectiveness of the proposed method on an Australian marine real data, and compare inverted results with check shot velocity information from a well.

INTRODUCTION

Conventional FWI is based on minimizing the misfit between predicted and observed data extracted from the wavefields at the sensor locations (Tarantola, 1984). Thanks to all the contributions made by researchers in our community, FWI has become a powerful tool to estimate high-resolution medium parameters granted we have a reasonably good initial models. Conventional l_2 norm least-squares measurement is not convex as a function of medium parameters. As a result, we cannot reach the global minimum when gradient-based optimizing methods are applied starting from a poor initial model when low-frequency components of the data are missing. Unlike conventional FWI aiming at minimizing data difference in a least-square sense subject to predicted data strictly following the wave equation, wavefield reconstruction inversion (WRI) relaxes the wave equation accuracy requirement allowing for better data fitting (Leeuwen and Herrmann, 2013). Although it can solve the cycle-skipping problem, it requires many relatively expensive iterations, as the model is updated at every iteration. To improve the computational efficiency of wavefield reconstruction, we utilize an efficient wavefield inversion (EWI) based on a modified source function that allows the wavefield to be inverted using a background velocity model. In this case, the inversion is divided into two steps, the wavefield construction, which we use to the calculate medium parameter perturbations using a direct division (deconvolution) method (Alkhalifah, 2019; Alkhalifah and Song, 2019).

However, ignoring the anisotropy of the true Earth results in poor results in many areas. Under this condition, a multi-parameter inversion is required to provide a better data fitting. For transversely isotropic media with a vertical axis of symmetry (VTI), the data sensitivity to the anisotropic parameters provides us with insights into the potenital tradeoff and optimal parametrization (Alkhalifah and Plessix, 2014). In the active seismic setup, Alkhalifah (2016) argues for an optimal parametrization for multi-parameter waveform inversion in VTI media with minimal tradeoff given by the horizontal velocity v_h, and the anisotropic parameters η and ε. In this parameterization, the horizontal velocity is initially reconstructed from the diving waves without worrying about the tradeoff from anisotropic parameters. Another parameterization using normal moveout (NMO) velocity, anisotropic parameters η and δ could also be effective for background updates (Djebbi et al., 2017).

In this abstract, we use EWI to apply a multi-parameter waveform inversion in an acoustic VTI medium setting. In the anisotropic case, the inversion of the primary (pressure) and auxiliary (perturbation) wavefields is mainly independent of the anisotropic parameters. Some of its scattering features will be embedded in the source functions. With a direct division, the medium parameter perturbations can be calculated directly, and the parameter tradeoff reduced. Application on a 2D real dataset shows the validity of the proposed method.

THEORY

We start by developing the inversion formulas for two sets of parameterizations we intend to use in the inversion of the marine dataset.

Parameterization: v_n, η, δ

We use a frequency domain VTI acoustic-wave equation with constant density to simulate the wave propagation considering the anisotropic nature of the Earth (Zhou et al., 2006). With a parameterization using the NMO velocity v_n and anisotropic parameters δ and η, the wave equation in 2D (x,z) is expressed as:

$$\begin{aligned} -\frac{\omega^2}{v_n^2}p-(\frac{\partial^2 p}{\partial x^2}+\frac{\partial^2 q}{\partial x^2})-\frac{1}{1+2\delta}\frac{\partial^2 p}{\partial z^2}=s,\\ -\frac{\omega^2}{v_n^2}q-2\eta(\frac{\partial^2 p}{\partial x^2}+\frac{\partial^2 q}{\partial x^2})=0, \end{aligned} \tag{1}$$

where, p is the pressure wavefield, and q is the perturbation wavefield. Here, ω denotes the angular frequency. The frequency domain VTI acoustic-wave equations can be expressed in compact form as:

$$\mathbf{L}(\mathbf{x},\omega)u(\mathbf{x},\omega)=f(\mathbf{x_s},\omega), \tag{2}$$

where, $\mathbf{L}(\mathbf{x},\omega)$ is the impedance matrix (modelling operator). $u(\mathbf{x},\omega)=[p\,q]^T$ represents the wavefield vector, and $f(\mathbf{x},\omega)=[s\;0]^T$ represents the source vector. $\mathbf{x}=(x,z)$ and $\mathbf{x_s}$ denote

the spatial dimensions and source locations. Conventionally, the wavefield u is calculated using the wave equation, which depends on the medium parameters. This dependency, demonstrated by the Born series, includes high non-linearity. In multi-parameter waveform inversion, we have an additional challenge. Since the data residuals could be caused by medium parameter, gradient-based optimization methods suffer from the tradeoff between different parameters. In order to solve these problems, we use EWI to implement a multi-parameter inversion in acoustic VTI media. The objective function of EWI is stated as:

$$E(u_i, f_{ei}) = min\frac{1}{2}\sum_i \|d_i - Cu_i\|_2^2 + \frac{\alpha}{2}\|\mathbf{L_0}u_i - f_{ei}\|_2^2, \quad (3)$$

where, i is the source index, and d_i is recorded data. α acts as a weighting factor on the background wave equation. At the beginning of the inversion process, we start with a background VTI modeling operator $\mathbf{L_0}$ corresponding to the background medium parameters: v_{n0}, δ_0, η_0. In the VTI acoustic-wave equation, wavefield $u = [p\ q]^T$ is made up of the pressure wavefield p and the perturbation wavefield q. In equation 3, the modified source function $f_e = [f_{es}\ f_{e0}]^T$ starts with the original source function $f = [s\ 0]^T$ in the inversion process. In order to make the data vector size consistent with the wavefield vector $u = [p\ q]^T$, we extend the data vector $d = [d_{obs}\ 0]^T$ by adding zero values at the end of observed data d_{obs}. This is valid for the marine case as our receivers are located in the isotropic water later where $q = 0$. However, for a general case, we utilize a mapping operator C that extracts values from the pressure wavefield q at the receiver positions and ignores the perturbation wavefield q which is an auxiliary function. In order to calculate the wavefield, which needs to simultaneously satisfy the data fitting objective and the wave equation, we minimize E by solving $\nabla_u E = 0$. Thus, the wavefield vector u is calculated by solving the following linear equation:

$$\begin{pmatrix} \alpha\mathbf{L_0} \\ C \end{pmatrix} u_i = \begin{pmatrix} \alpha f_{ei} \\ d_i \end{pmatrix}. \quad (4)$$

We solve this linear equation using a least-squares optimization. As a result, the initial pressure wavefield p and the perturbation wavefield q in the model space using the background medium parameters are reconstructed. The modified source function which satisfies the wave equation using the background operator is calculated as:

$$f_e = \mathbf{L_0}u. \quad (5)$$

This background-medium wavefield will include only single scattered energy from the missing perturbations. Inner iterations between 4 and 5 will add multi-scattering components into the reconstructed wavefield. As parameter perturbations include multi-scattering components, the convergence rate in each parameter inversion accelerates. In each frequency, the background operator $\mathbf{L_0}$ stays stationary, so only one LU decomposition is required. Cheap inner iterations only add little cost. We set $m_n = \frac{1}{v_n^2}$, $\zeta = \frac{1}{1+2\delta}$, and define the initial (background) medium parameters with m_{n0}, ζ_0 and η_0. Using background medium parameters, equation 1 is expressed as:

$$\begin{aligned} -\omega^2 m_{n0}\, p - (\frac{\partial^2 p}{\partial x^2} + \frac{\partial^2 q}{\partial x^2}) - \zeta_0\frac{\partial^2 p}{\partial z^2} &= f_{es}, \\ -\omega^2 m_{n0}\, q - 2\eta_0(\frac{\partial^2 p}{\partial x^2} + \frac{\partial^2 q}{\partial x^2}) &= f_{e0}. \end{aligned} \quad (6)$$

The modified source function $f_e = [f_{es}\ f_{e0}]^T$ satisfies the wave equation using the background operator. Using the new f_e, we can solve for the wavefield again to include multi scattered energy. We define parameter perturbations as δm_n, $\delta\zeta$, and $\delta\eta$, so the true models are given by:

$$m_n = m_{n0} + \delta m_n;\ \zeta = \zeta_0 + \delta\zeta;\ \eta = \eta_0 + \delta\eta. \quad (7)$$

Plugging equation 7 into equation 1 and subtracting equation 6, we get the relations between the medium parameter perturbations and the modified source as follows:

$$\begin{aligned} s + \omega^2\delta m_n\, p + \delta\zeta\frac{\partial^2 p}{\partial z^2} &= f_{es}, \\ \omega^2\delta m_n\, q + 2\delta\eta(\frac{\partial^2 p}{\partial x^2} + \frac{\partial^2 q}{\partial x^2}) &= f_{e0}, \end{aligned} \quad (8)$$

In our implementation, we use a sequential inversion in the order of v_n, η, δ. The medium parameter perturbations of δm, $\delta\zeta$ and $\delta\eta$ can be calculated using direct division as:

$$\delta m_n = \Re[\frac{p^*(s - f_{es})}{\omega^2 p^* p + \lambda}], \quad (9)$$

$$\delta\zeta = \Re[\frac{w^*(s - f_{es})}{\omega^2 w^* w + \lambda}], \quad (10)$$

$$\delta\eta = \Re[\frac{r^* f_{e0}}{\omega^2 r^* r + \lambda}], \quad (11)$$

where, λ has a small value to avoid dividing over zero, $w = \frac{\partial^2 p}{\partial z^2}$, and $r = \frac{\partial^2 p}{\partial x^2} + \frac{\partial^2 q}{\partial x^2}$. After obtaining the parameter perturbations δm, $\delta\zeta$ and $\delta\eta$, we update the background model using equation 7.

Parameterization: v_h, η, ε

As the horizontal velocity v_h, the NMO velocity v_n, and Thomsen anisotropy parameters δ, η, ε have the following relations:

$$v_h = v_n\sqrt{1+2\eta},\ 1+2\delta = \frac{1+2\varepsilon}{1+2\eta}, \quad (12)$$

we re-parameterize the VTI acoustic-wave equation 1 using the horizontal velocity v_h and anisotropic parameters ε and η. As a result, the VTI acoustic-wave equation is given by:

$$\begin{aligned} -\frac{\omega^2}{v_h^2}p - \frac{1}{1+2\eta}(\frac{\partial^2 p}{\partial x^2} + \frac{\partial^2 q}{\partial x^2}) - \frac{1}{1+2\varepsilon}\frac{\partial^2 p}{\partial z^2} &= s, \\ -\frac{\omega^2}{v_h^2}q - (\frac{\partial^2 p}{\partial x^2} + \frac{\partial^2 q}{\partial x^2}) + \frac{1}{1+2\eta}(\frac{\partial^2 p}{\partial x^2} + \frac{\partial^2 q}{\partial x^2}) &= 0, \end{aligned} \quad (13)$$

We set $m_h = \frac{1}{v_h^2}$, $\xi = \frac{1}{1+2\eta}$, $\mu = \frac{1}{1+2\varepsilon}$, and perturb each medium parameter by δm, $\delta\xi$ and $\delta\mu$. Using the background medium parameters, equation 14 is expressed as:

$$\begin{aligned} -\omega^2 m_{h0}\, p - \xi_0(\frac{\partial^2 p}{\partial x^2} + \frac{\partial^2 q}{\partial x^2}) - \mu_0\frac{\partial^2 p}{\partial z^2} &= f_{es}, \\ -\omega^2 m_{h0}\, q - (\frac{\partial^2 p}{\partial x^2} + \frac{\partial^2 q}{\partial x^2}) + \xi_0(\frac{\partial^2 p}{\partial x^2} + \frac{\partial^2 q}{\partial x^2}) &= f_{e0}, \end{aligned} \quad (14)$$

Like what we did previously, we subtract equation 14 from equation 13, and we get the relations between medium parameter perturbations and the modified source. The medium parameter perturbations of δm_h, $\delta\xi$ and $\delta\mu$ are calculated using:

$$\delta m_h = \Re[\frac{p^*(s-f_{es})}{\omega^2 p^* p+\lambda}], \tag{15}$$

$$\delta\mu = \Re[\frac{w^*(s-f_{es})}{w^* w+\lambda}], \tag{16}$$

$$\delta\xi = \Re[\frac{r^* f_{e0}}{r^* r+\lambda} + \frac{r^*(s-f_{es})}{r^* r+\lambda}], \tag{17}$$

where, $w = \frac{\partial^2 p}{\partial z^2}$ and $r = \frac{\partial^2 p}{\partial x^2} + \frac{\partial^2 q}{\partial x^2}$. In the two sets of parameterizations, the only difference in their updates is related to the parameter η in equations 11 and 17. While for equation 11, the update clearly relies on horizontally traveling waves, the update provided by equation 17 is focused on a narrow band at 45 degrees, as reflected also in the radiation pattens we share later in the abstract.

EXAMPLES

This 2-D marine dataset is from North-Western Australia Continental Shelf, acquired by CGG using a Broadseis acquisition system with a variable depth streamer (Soubaras and Dowle, 2010). Frequencies below 2.5 Hz has been filtered out due to the poor signal-to-noise ratio (SNR). One example shot gather is shown in Figure 1. The original dataset contains 1824 shot gathers at an interval of approximately 0.01875 km, we choose only 100 shot gathers corresponding to the 2D survey area of interest. The target model area we choose is 12.5 km long and 3.75 km in depth. The initial horizontal velocity model is borrowed from (Kalita and Alkhalifah, 2017, 2018), as shown in Figures 2.

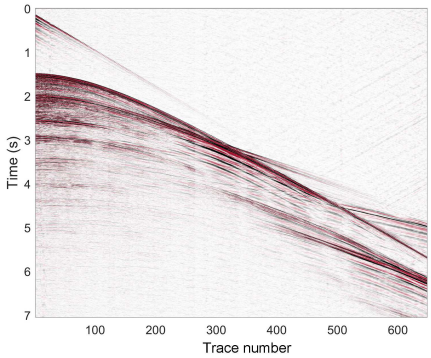

Figure 1: One shot gather of the real dataset.

We resample the data and use 324 receivers, with an interval of 0.025 km. Firstly, we perform an isotropic EWI in two stages by a hierarchal approach. In stage 1, we invert for the selected frequency band from 3 Hz to 6 Hz with a dense sampling of 0.15 Hz. In stage 2, the selected frequency band is from 9 Hz to 12 Hz. We use two inner iterations within each frequency and

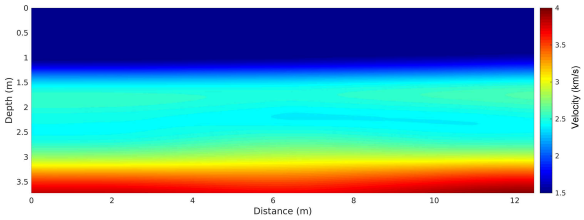

Figure 2: Initial velocity model.

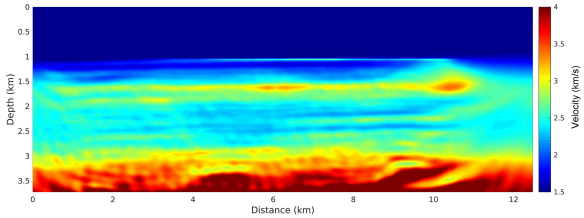

Figure 3: Inverted velocity using isotropic EWI.

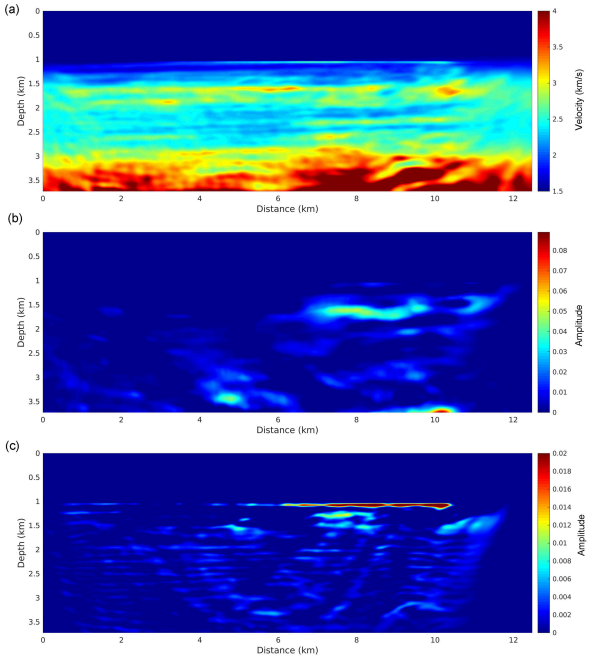

Figure 4: NMO velocity v_n (a), η (b), and δ (c).

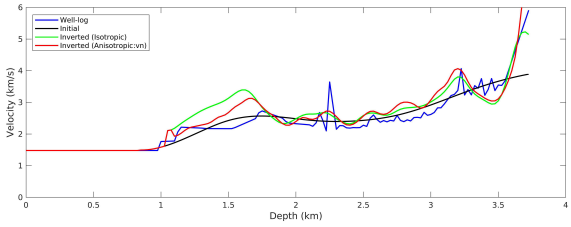

Figure 5: NMO velocity profile at 10.5 km.

two outer iterations over the frequencies of each stage. The α used here is set to $10e^8$. The inversion result is shown in Fig. 3. It is obvious that more detailed high-resolution information is recovered in the velocity model, especially in low velocity layers between 2.0 km to 2.5 km depth. Next, we perform an anisotropic EWI using the same inversion setup and strategy. We use the isotropic inverted velocity model as the initial velocity, and set initial anisotropic parameters to zero. With the parameterization of v_n, η, δ, the inverted NMO velocity v_n, η, and δ are shown in Figures 4a, 4b, and 4c, respectively. In the inverted η, we capture a smooth anisotropic behaviour in the shallow part of the model as shown in Figure 4b. The δ model attracts the high-wavenumber reflectivity-like information, as shown in Figure 4c. As expected, we are not able to invert for background δ information. From the velocity profile shown in Figure 5, we observe that the sequentially inverted NMO velocity fits the well-log (vertical) velocity better than the initially inverted velocity from isotropic EWI. Actually, the difference between the two velocities can be used to extract background δ information. We also test anisotropic EWI with the parametrization using (v_h, η, ε) with the same setup. The inverted horizontal velocity, η, and ε are shown in Figures 6a, 6b, and 6c, respectively. Similarly, we see that low-wavenumber η is recovered in the shallow part, while high-wavenumber ε is recovered throughout. Figure 7 shows that the inverted horizontal velocity is close to true velocity well. As expected, we notice that the horizontal velocity is higher than the NMO velocity (Figure 4a), which reflects background η. The radiation patterns of both two parameterizations are shown in Figures 8a and 8b. They provide the theoretical insights into the resolved parameters. The NMO and horizontal velocities have angle independent radiation patterns. δ and ε are more sensitive to small scattering angles which correspond to reflection waves. η is mainly provided by large scattering angles or large offsets when NMO velocity is used. By comparison, η has much lower sensitivity when horizontal velocity is used, and it can only be recovered partially in the shallow part.

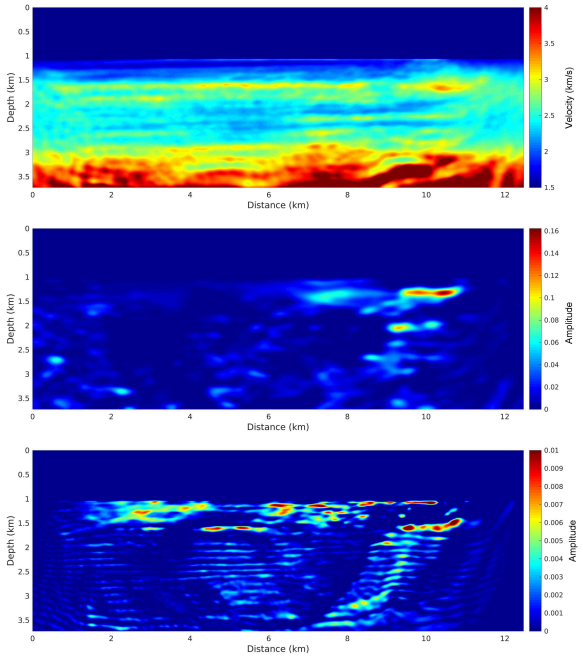

Figure 6: Horizontal velocity v_h (a), η (b), and ε (c).

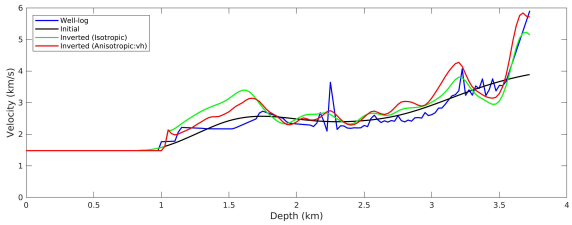

Figure 7: Horizontal velocity profile at 10.5 km.

CONCLUSIONS

We apply an efficient wavefield inversion for multi-parameters in acoustic VTI media using various parameterizations on a marine dataset. The parameterization allows us to invert for the three medium parameters in a sequential matter. As the model perturbations are calculated using direct division, it reduces the tradeoff in the multi-parameter inversion.

ACKNOWLEDGMENTS

We thank KAUST for sponsoring this research. We thank our SWAG colleagues for their helpful suggestions, especially Mahesh Kalita for providing the initial velocity model. This work utilized the resources of the Supercomputing Laboratory at King Abdullah University of Science and Technology (KAUST) in Thuwal, Saudi Arabia, and we are grateful for that.

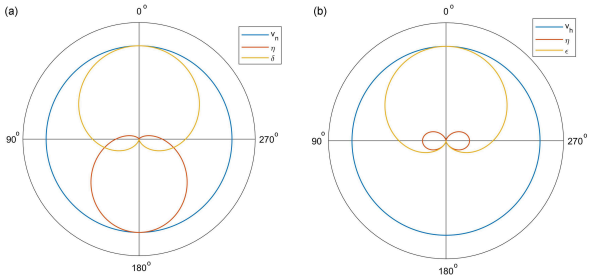

Figure 8: Radiation patterns for the parametrizations:(v_n, η, δ) (a) and (v_h, η, ε) (b).

REFERENCES

Alkhalifah, T., 2016, Research note: Insights into the data dependency on anisotropy: An inversion prospective: Geophysical Prospecting, **64**, 505–513.

———, 2019, Linear wavefield optimization using a modified source: Communications in computational physics, accepted.

Alkhalifah, T., and R.-É. Plessix, 2014, A recipe for practical full-waveform inversion in anisotropic media: An analytical parameter resolution study: Geophysics, **79**, R91–R101.

Alkhalifah, T., and C. Song, 2019, An efficient wavefield inversion: 81th EAGE Conference and Exhibition 2019.

Djebbi, R., R.-É. Plessix, and T. Alkhalifah, 2017, Analysis of the traveltime sensitivity kernels for an acoustic transversely isotropic medium with a vertical axis of symmetry: Geophysical prospecting, **65**, 22–34.

Kalita, M., and T. Alkhalifah, 2017, Efficient full waveform inversion using the excitation representation of the source wavefield: Geophysical Journal International, **210**, 1581–1594.

———, 2018, Multiscale full-waveform inversion using flux corrected transport: 1153–1157.

Leeuwen, T. V., and F. Herrmann, 2013, Mitigating local minima in full-waveform inversion by expanding the search space: Geophysical Journal International, **195**, 661–667.

Soubaras, R., and R. Dowle, 2010, Variable-depth streamer–a broadband marine solution: first break, **28**.

Tarantola, A., 1984, Inversion of seismic reflection data in the acoustic approximation: Geophysics, **49**, 1259–1266.

Zhou, H., G. Zhang, and R. Bloor, 2006, An anisotropic acoustic wave equation for vti media: 68th EAGE Conference and Exhibition incorporating SPE EUROPEC 2006, H033.